energies

MDPI

Article

In Situ Growth of COF on PAN Nanofibers to Improve Proton Conductivity and Dimensional Stability in Proton Exchange Membranes

Xiaoyu Meng [1,2,*], Yinan Lv [1], Jihong Wen [1], Xiaojing Li [1], Luman Peng [1], Chuanbo Cong [1,2], Haimu Ye [1,2] and Qiong Zhou [1,2]

[1] Department of Materials Science and Engineering, College of New Energy and Materials, China University of Petroleum, Beijing 102249, China; lvyinan11011@163.com (Y.L.); wenjihong2006@163.com (J.W.); lixj9705@163.com (X.L.); plm199810@163.com (L.P.); congcb@cup.edu.cn (C.C.); yehaimu@cup.edu.cn (H.Y.); zhouqiong_cn@163.com (Q.Z.)

[2] Beijing Key Laboratory of Failure, Corrosion, and Protection of Oil/Gas Facilities, China University of Petroleum, Beijing 102249, China

* Correspondence: mengxy@cup.edu.cn

Abstract: Perfluorosulfonic acid (PFSA) polymer is considered as a proton exchange membrane material with great potential. Nevertheless, excessive water absorption caused by abundant sulfonic acid groups makes PFSA have low dimensional stabilities. In order to improve the dimensional stability of PFSA membranes, nanofibers are introduced into PFSA membranes. However, because nanofibers lack proton conducting groups, it usually reduces the proton conductivities of PFSA membranes. It is a challenge to improve dimensional stabilities while maintaining high proton conductivities. Due to the structural designability, covalent organic frameworks (COFs) with proton conductive groups are chosen to improve the overall performance of PFSA membranes. Herein, COFs synthesized in situ on three-dimensional PAN nanofibers were introduced into PFSA to prepare PFSA@PAN/TpPa-SO_3H sandwiched membranes. The PFSA@PAN/TpPa-SO_3H-5 composite membrane exhibited outstanding proton conductivity, which reached 260.81 mS·cm^{-1} at 80 °C and 100% RH, and only decreased by 4.7% in 264 h. The power density of a single fuel cell with PFSA@PAN/TpPa-SO_3H-5 was as high as 392.7 mW·cm^{-2}. Compared with the pristine PFSA membrane, the conductivity of PFSA@PAN/TpPa-SO_3H-5 increased by 70.0 mS·cm^{-1}, and the area swelling ratio decreased by 8.1%. Our work provides a novel strategy to prepare continuous proton transport channels to simultaneously improve conductivities and dimensional stabilities of proton exchange membranes.

Keywords: electrospinning; perfluorosulfonic acid; nanofibers; covalent organic frameworks; proton exchange membranes; fuel cell; polyacrylonitrile; dimensional stability

Citation: Meng, X.; Lv, Y.; Wen, J.; Li, X.; Peng, L.; Cong, C.; Ye, H.; Zhou, Q. In Situ Growth of COF on PAN Nanofibers to Improve Proton Conductivity and Dimensional Stability in Proton Exchange Membranes. *Energies* **2022**, *15*, 3405. https://doi.org/10.3390/en15093405

Academic Editors: Dan Luo, Yujia Lv and Shengwei Zhang

Received: 11 April 2022
Accepted: 3 May 2022
Published: 6 May 2022

1. Introduction

A proton exchange membrane (PEM) is the core component of a proton exchange membrane fuel cell (PEMFC), and provides a channel for the migration and transportation of protons [1]. Its quality directly affects the service life of the battery [2,3]. Perfluorosulfonic acid (PFSA) proton exchange membranes are composed of hydrophobic main chains of polytetrafluoroethylene (PTFE) and hydrophilic side chains of sulfonic acid. PFSA membranes are rich in hydrophilic ionic groups and are easily hydrated. Therefore, perfluorosulfonic acid membranes have outstanding proton conductivities. Nafion, produced by DuPont, is widely used as a proton exchange membrane [4]. However, PEMs often work in high temperature environments, and the unavoidable changes of relative humidity will cause aqueous polyelectrolytes to undergo rapid water absorption or dehydration. This process is accompanied by dimensional expansion or shrinkage, causing the catalytic layer to peel off from PEMs and fuel cell performance will degradate [5]. Therefore, it is of vital

importance to improve the dimensional stability of polymer electrolyte membranes while maintaining high proton conductivities.

In recent years, with the maturity of electrospinning technology, compounding with three-dimensional fibers became an effective method to improve the dimensional stability [6–8], and other properties such as improved mechanical properties due to friction between fibers [9,10]. When the interface of nanofibers and ionomers is compatible, the fibers will limit the water absorption of composite membranes and improve the dimensional stability [11]. Although the dimensional stabilities of the proton exchange membranes are improved after the introduction of fibers, the addition of fibers will reduce the conductivities of composite membranes due to the lack of conductive groups [7,12–14]. Therefore, the modification of nanofibers has become a research hotspot. Although fiber modification can improve the proton conductivities of PEMs, this strategy will sacrifice fiber stability, resulting in an inefficient effect of the fibers on the dimensional stabilities of PEMs. For instance, phytic-acid-loaded PBI nanofibers significantly enhanced the proton conductivity of PEMs with a Nafion matrix. This effect is more obvious with the increase in phytic acid content. The addition of more phytic acid also significantly reduced the improvement of PBI nanofibers on the dimensional stability of PEMs [15]. L-lysine-modified PAN fibers can simultaneously improve the proton conductivity and dimensional stability of Nafion. When higher proton conductivity is required, the loading of L-lysine is higher, and the dimensional stability of PEMs is only slightly improved [16]. Therefore, loading conductive particles on the surface of nanofibers can be a very effective method to simultaneously improve proton conductivity and dimensional stability. Zhuang et al., attached a zeolitic imidazolate framework (ZIF-8), a commonly chosen metal-organic framework (MOF), to the surface of poly (m-phthaloyl-m-phthalamide) nanofibers (PMIA NFs) by a hydrothermal method and combined with Nafion to construct continuous proton nanochannels. At 80 °C and 100% RH, the composite membrane showed a conductivity of 0.258 $S \cdot cm^{-1}$. In addition, the fiber composite membrane had excellent thermal stability and dimensional stability [17].

However, due to the low compatibility of MOFs with polymer matrices, MOF-modified polymer composite membranes are prone to defects, and thus the proton conductivities or dimensional stabilities of the membranes will be reduced [18]. A covalent organic framework (COF) is a crystalline porous material with good compatibility with polymer matrices, with excellent structural stability [19–21]. Abundant functional groups and ordered pores make COFs as composite materials of fillers and polymer matrices, which can effectively improve the proton conductivities, dimensional stabilities and battery performances of proton exchange membranes [22–25]. Yin et al., added TpPa-SO_3H nanosheets to a SPEEK matrix to prepare composite PEMs. The maximum proton conductivity of the SPEEK/TpPa-SO_3H-5 membrane was 0.346 $S \cdot cm^{-1}$, and the dimensional stabilities of SPEEK matrix membranes were improved [26]. The traditional preparation of COFs/fiber composite structures by electrospinning is usually divided into the following two steps: (a) mixing COF nanoparticles with a polymer to form a uniform solution; (b) converting the solution into continuous fibers by electrospinning. Since the COF nanoparticles are covered by the polymer, the surface area and active sites of the fibers obtained by the traditional method are significantly reduced, and the COFs cannot effectively form a continuous channel. Growing COFs on fiber surfaces by in situ synthesis can solve the above problems. Constructing continuous fibrous COFs and applying them to various structural equipment is a long-term goal.

Herein, we prepared polyacrylonitrile nanofibers with TpPa-SO_3H (PAN/TpPa-SO_3H) grown on the nanofibers surface by in situ synthesis. The –SO_3H on the surface of PAN/TpPa-SO_3H greatly increases the concentration of –SO_3H in PEMs, and the interaction between –NH_2 and –SO_3H of PFSA can induce active groups as proton transfer sites to aggregate along the nanofiber, thereby achieving effective proton conduction. PAN/TpPa-SO_3H was then inserted into two PFSA layers to form a "sandwich" structure PEM. The backbone of PAN/TpPa-SO_3H can inhibit the swelling of PFSA,

thereby improving dimensional stability. All in all, we have successfully manufactured PFSA@PAN/TpPa-SO_3H PEMs with remarkable proton conductivities, conductivity stabilities, and dimensional stabilities.

2. Materials and Methods

2.1. Materials

Polyacrylonitrile (PAN) with the molecular weight of 150,000 was produced by Shanghai Macklin Biochemical Co., Ltd., Shanghai, China. N,N-dimethylformamide (DMF, AR, 99.5%) 1,3,5-triformylphloroglucinol (Tp, 97%), 2,5-diaminobenzenesulfonic acid (Pa-SO_3H, >98%) and p-Toluenesulfonic acid (PTSA, 99%) were produced by Aladdin Biochemical Technology Co., Ltd., China. PFSA (~10.5 wt% solution; solvents: 45.5 wt% ethanol, and 44 wt% water; equivalent weight: 900 g/mol) was produced by DongYue Federation, China. The other reagents mentioned in this work were produced by Beijing chemical reagent factory, China.

2.2. Preparation of PAN/TpPa-SO_3H Nanofibers

Firstly, 0.2 g PAN and 1,3,5-triformylm-triphenol (Tp) were dissolved in 1.8 g DMF at a ratio of 10:x (x = 1, 3, 5, 7). After stirring for 12 h at 25 °C, the uniform spinning solution was spun at 13 kV positive voltage with a bolus speed of 0.08 mm/min and a receiving distance of 15 cm to obtain PAN/Tp nanofibers. Secondly, 0.3 g of p-toluenesulfonic acid (PTSA) and 0.05 g of diaminobenzenesulfonic acid (Pa-SO_3H) were added to 15 mL of deionized water, and ultrasonicated for 10 min to prepare a homogeneous reaction solution. The PAN nanofibers were cut into sizes of 6 × 6 cm and put into the reaction solution. Then reacted at 90 °C for 3 days to synthesize TpPa-SO_3H on the surface of PAN to prepare PAN/TpPa-SO_3H-x (the synthesized COFs are recorded as TpPa-SO_3H-x. The value of x depends on the amount of Tp, x = 1, 3, 5, 7). The PAN/TpPa-SO_3H nanofibers were placed in a beaker containing 50 mL of deionized water 3 times for 20 s, and then washed in 50 mL of deionized water several times to remove unreacted Pa-SO_3H and PTSA. After drying at 60 °C for 6 h, the PAN/TpPa-SO_3H nanofibers were obtained.

2.3. Membrane Preparation

In total, 1 g of ethylene glycol (EG) was added to 9 g of 10 wt% PFSA solution to prepare a 9 wt% uniform solution. A total of 5 g of PFSA/EG solution was poured into a glass mold and the PAN/TpPa-SO_3H nanofibers were spread on the surface of the EG/PFSA solution. Then, the remaining 5 g of EG/PFSA solution on the surface of the nanofibers was covered evenly at 80 °C and treated in an oven for 72 h, and then heat-treated at 140 °C for 2 h to obtain the PFSA@PAN/TpPa-SO_3H composite membranes. PFSA membranes and PFSA@PAN composite membranes were prepared by the same method as the control group. All composite membranes were prepared by solution casting.

2.4. Characterization

Morphology of nanofibers and the cross-sections were characterized using a scanning electron microscope (SEM) (HITACHI SU8010, Tokyo, Japan). The structure of TpPa-SO_3H was characterized by the Fourier transform infrared spectroscopy (FTIR, Bruker Tensor II, Bremen, Germany), 13C solid state nuclear magnetic resonance (SSNMR, JNM ECZ600R, Japan), and X-ray photoelectron spectroscopy (XPS, Thermo Scientific K-Alpha, Waltham, MA, USA). The pore structure was characterized by a N_2 adsorption-desorption method (ASAP 2460 3.01, Shanghai, China). The mechanical properties were measured by a universal tensile testing machine (KQL, WDL-10, Yangzhou, China). Thermogravimetric analysis was used to characterize the thermal stability of membranes (SHIMADZU DTG-60, Japan). Proton conductivities were characterized by an electrochemical workstation (Shanghai Chenhua CHI670D, Shanghai, China). Thermal stability was tested by thermogravimetric analysis (TGA, TA Q5000, New Castle, DE, USA). The oxidative stability of the membranes was tested by weighing the residual mass ratio of the membranes after immersion in

Fenton's reagent at 80 °C for 24 h (configure 3 ppm Fe^{2+} solution, then add H_2O_2, and configure the solution into a solution containing 3wt% H_2O_2 to obtain Fenton's reagent). The fuel cell performance was characterized by Fuel Cell Test System 850e. The positive and negative electrodes of membrane electrode assemblies were loaded with a Pt/C catalyst of 0.5 g/cm^2. All the membranes were tested at 80 °C in an environment where the humidity of both H_2 and O_2 was 100%. The back pressure during the test was 1 atm (~0.1 MPa). Both H_2 and O_2 have a gas flux of 150 SCCM.

2.5. Water Uptaking and Swelling Ratio

The water absorption and area swelling ratio of the film can be determined by the difference between the weight of the sample in a completely dry state (W_{dry} and S_{dry}) and the weight of the sample in a completely hydrated state (W_{wet} and S_{wet}) at different temperatures. The specific steps are as follows: cut the dried film sample into a rectangle (about 1 cm × 3 cm), and record its mass (W_{dry}) and area (S_{dry}). Then, the samples were immersed in deionized water at different temperatures for 12 h. After that, the moisture on the surface of the membrane was quickly removed using a water-absorbing material (such as filter paper), and then the wet weight (W_{wet}) and wet area (S_{wet}) of the membrane was quickly measured. Each sample was measured at least three times and the average value calculated. The water absorption and swelling degree of the film was calculated by the following formula:

$$\text{Water Uptaking } (\%) = \frac{\left(W_{wet} - W_{dry}\right)}{\left(W_{dry}\right)} \quad (1)$$

$$\text{Area swelling ratio } (\%) = \frac{\left(S_{wet} - S_{dry}\right)}{\left(S_{dry}\right)} \quad (2)$$

2.6. Proton Conductivity

The proton conductivity was characterized by CHI670D. The test was carried out under different temperature and relative humidity (RH) conditions in the YSGTS-50 constant temperature and humidity test chamber. All membrane samples were cut into 1.5 cm × 3 cm sample strips before the test and placed in a constant temperature and humidity test chamber to be sufficiently stable under the tested conditions. The proton conductivity of the membrane was calculated according to Equation (3):

$$\sigma = \frac{L}{AR} \quad (3)$$

where σ represents the proton conductivity of the membrane (mS·cm^{-1}), L is the distance between the two platinum electrodes (cm), R (Ω) is the resistance value of the membrane, and A is the cross-sectional area of samples.

3. Results and Discussion

3.1. Characterization of the In Situ PAN/TpPa-SO_3H Nanofibers

The microstructure of the composite nanofibers was characterized by SEM, as shown in Figure 1. In the SEM images of PAN/TpPa-SO_3H, TpPa-SO_3H was in the form of small spheres, covering the fiber surfaces. As the ratio of Tp increased, the loading of TpPa-SO_3H on the fiber surface gradually increased. As shown in Figure 1f, when the ratio of PAN:Tp was 10:5, the TpPa-SO_3H loading reached the maximum value of 31.6%. Then with the increase in the proportion of Tp to PAN, the TpPa-SO_3H load no longer increased significantly. From an economic point of view, 10:5 was the most appropriate ratio of PAN:Tp.

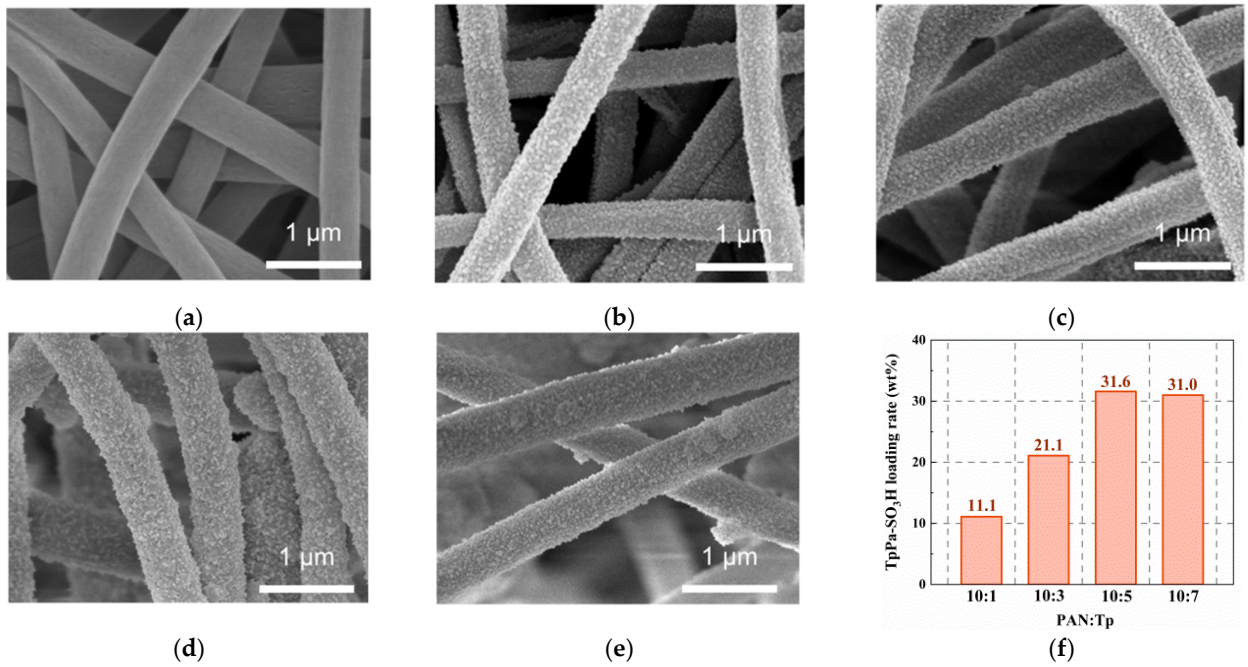

Figure 1. The SEM images of PAN and PAN/TpPa-SO_3H nanofibers: (**a**) PAN, (**b**) PAN:Tp = 10:1, (**c**) 10:3, (**d**) 10:5 and (**e**) 10:7 after reaction at 90 °C for 3 days, respectively; (**f**) TpPa-SO_3H loading on nanofiber surface of different PAN:Tp ratio.

The surface structure of the PAN/TpPa-SO_3H fiber membrane was characterized by FTIR. As shown in Figure 2a, the disappearance of the N-H bond between 3425 and 3334 cm^{-1}, the C=OH bond at 2927 cm^{-1}, and the C=O bond at 1659 cm^{-1} indicate that the precursor reactants of TpPa-SO_3H were completely consumed by the Schiff base reaction [27,28]. The presence of C=C bonds at 1583 cm^{-1}, C-N bonds at 1231 cm^{-1}, and S-OH bonds at 1020 cm^{-1} indicated that TpPa-SO_3H was successfully synthesized on the PAN fibers [24,29]. The peak enhanced with the increasing content of TpPa-SO_3H loaded on the surface of the nanofiber.

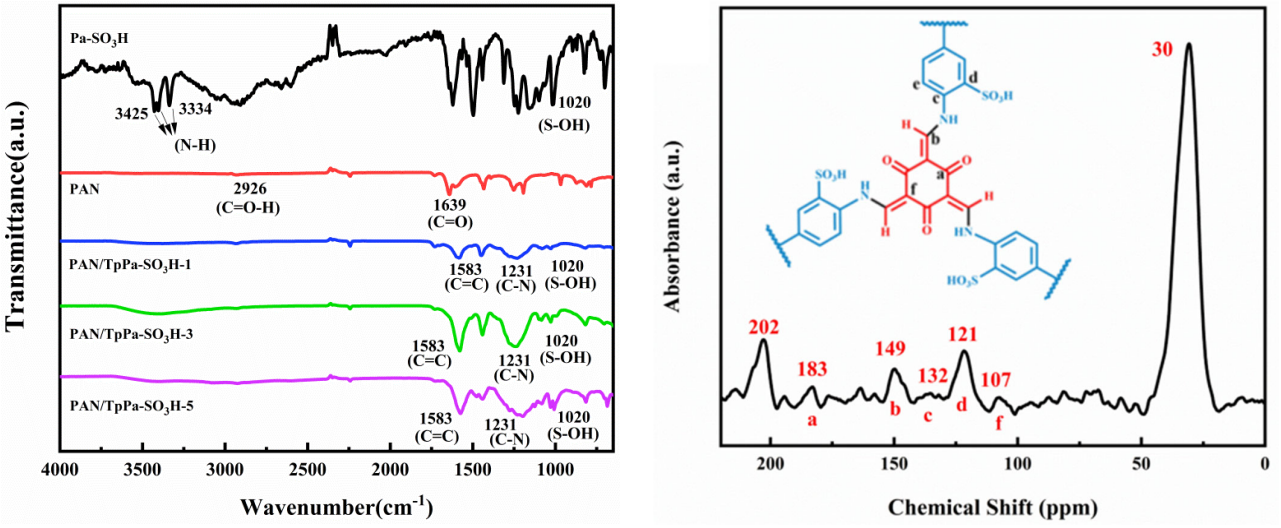

Figure 2. (**a**) FTIR image of Pa-SO_3H, PAN and PAN/TpPa-SO_3H with different ratio of Tp:PAN. (**b**) Solid state 13C CP-MAS spectrum comparison of PAN/TpPa-SO_3H.

In addition, a 13C SSNMR test was carried out, and the results are shown in Figure 2b. The NMR spectrum of TpPa-SO_3H has three typical resonances around 183 ppm, 149 ppm and 107 ppm. The resonance at 183 ppm corresponds to the carbon atom on the secondary amine group, indicating the existence of typical keto-enol tautomers. The resonances of carbon atoms on the aromatic ring resulting from the ketone-enol mutation are around 107 ppm. The resonance peak around 132 ppm corresponds to the carbon atom attached to the secondary amine group on the benzene ring. The signal around 121 ppm corresponds to carbon atoms near the sulfonic acid group [28,30]. The peak at 30 ppm is the secondary and tertiary carbon of PAN.

XPS analysis was performed on PAN/TpPa-SO_3H to further investigate the compositions. As shown in Figure 3a, the N1s binding energy of TpPa-SO_3H showed two types of nitrogen: one is a free secondary amine (-NH) of 400.2 eV, and the other is a protonated secondary amine (-NH^{2+}) of 402.3 eV. Figure 3b shows that the binding energy peak of S2p of PAN/TpPa-SO_3H. The binding energies of 168.0 eV and 169.3 eV, respectively, originate from -SO_3^- and -SO_3H, indicating that the synthesized substance contained -SO_3H. The combination of FTIR and XPS showed that TpPa-SO_3H was successfully synthesized on the surface of PAN.

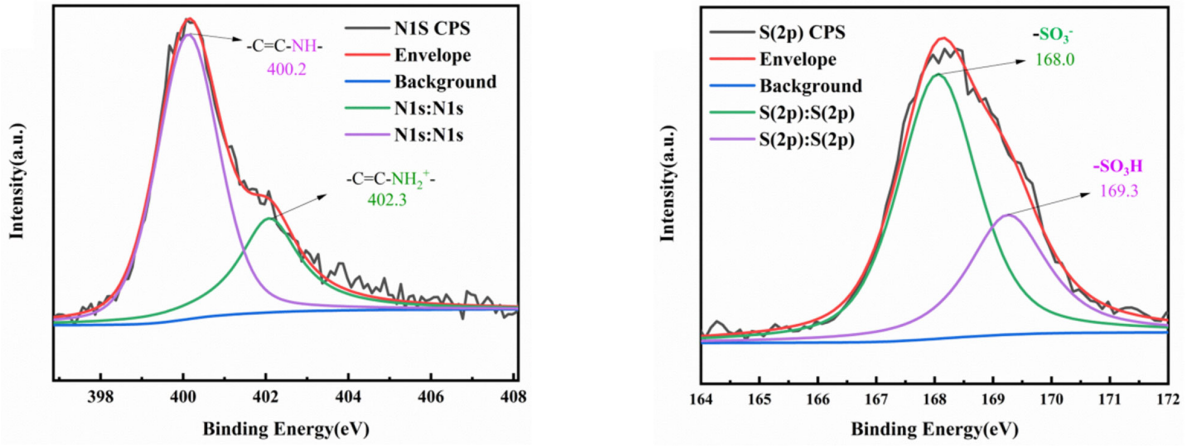

(**a**) (**b**)

Figure 3. XPS spectra of the PAN/TpPa-SO_3H nanofibers. Binding energy of (**a**) N1s and (**b**) S2p for TpPa-SO_3H.

As shown in Figure 4, the pore structure was characterized by N_2 adsorption-desorption method. The obvious type IV hysteresis loop indicates that PAN/TpPa-SO_3H had mesoporous structures. The BET surface areas of PAN and PAN/TpPa-SO_3H were 6.37 and 78.25 $m^2 \cdot g^{-1}$, respectively. Compared with PAN, the BET surface area of PAN/TpPa-SO_3H was significantly increased. It is shown that the PAN/TpPa-SO_3H prepared by in situ synthesis method can exhibit high surface area, which can improve the absorption efficiency.

3.2. Characterization of Nanofiber Composite Membranes

PAN/TpPa-SO_3H also exhibited an excellent solvent resistance stability in PFSA solution. Cross-sectional SEM proved the excellent combination of PAN/TpPa-SO_3H and PFSA. Figure 5 showed the SEM images of the cross-section of the PFSA membrane and the composite membrane. The PFSA membrane structure was uniform and dense. In PFSA@PAN composite membranes, the PAN nanofiber has good compatibility with the PFSA matrix, and there was no obvious delamination. Figure 5c–e are SEM images of membranes with different ratios of TpPa-SO_3H. According to the SEM of the cross-section for composite membranes, heterogeneous fibers can be clearly observed in PFSA@PAN/TpPa-SO_3H. Compared with PFSA@PAN, the PFSA@PAN/TpPa-SO_3H composite membranes are grainy. With the increase in TpPa-SO_3H content, there was no incompatibility or delamination between PFSA matrix and PAN/TpPa-SO_3H layer. The absence of voids between

the fiber and the substrate indicated an excellent compatibility between PAN/TpPa-SO_3H and PFSA.

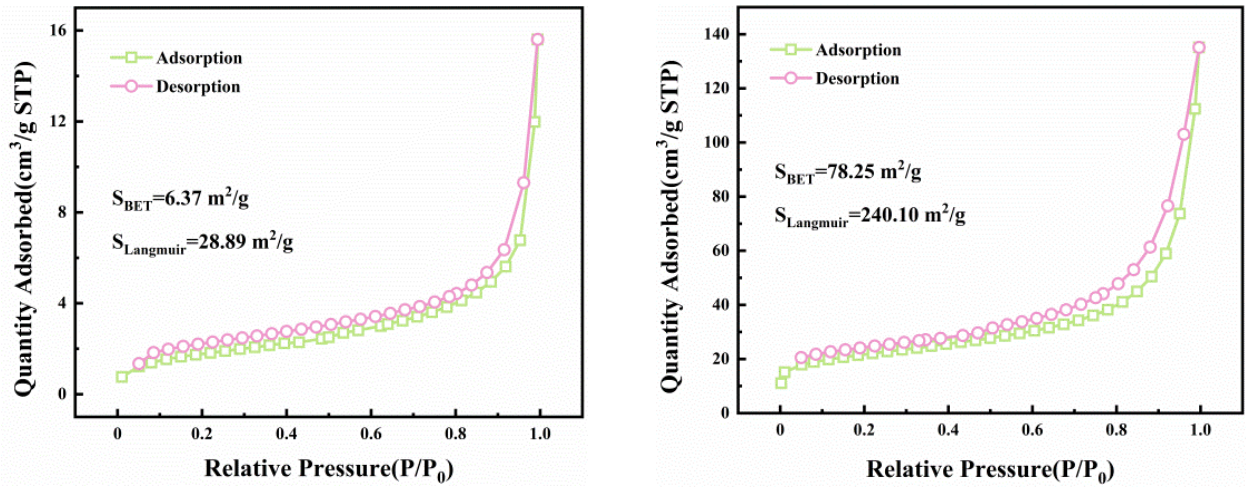

Figure 4. N_2 adsorption and desorption measurements and pore size distribution of (**a**) PAN and (**b**) PAN/TpPa-SO_3H at 77 K.

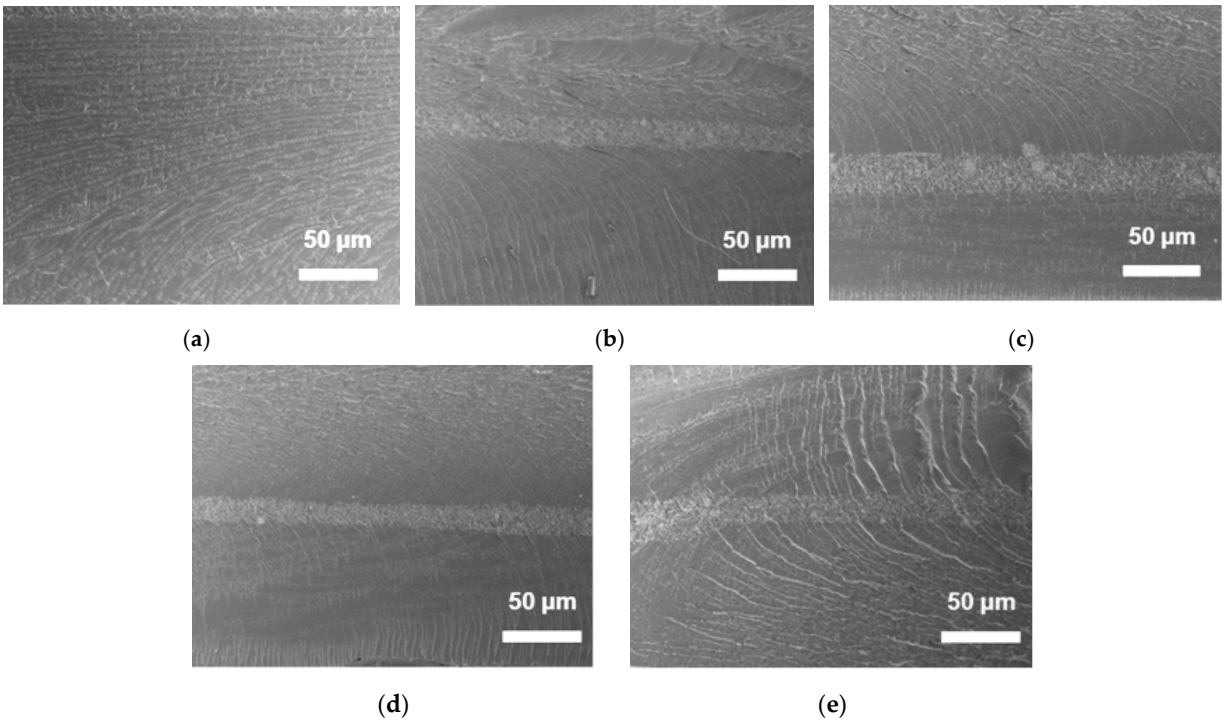

Figure 5. Cross-sectional SEM images of (**a**) PFSA, (**b**) PFSA@PAN, (**c**) PFSA@PAN/TpPa-SO_3H-1, (**d**) PFSA@PAN/TpPa-SO_3H-3, and (**e**) PFSA@PAN/TpPa-SO_3H-5.

3.3. Water Uptaking and Area Swelling Ratio

Water uptaking and area swelling play important roles in characterizing proton conductivity and dimensional stability of PEMs. H_2O can be used as a proton transport carrier, but it will reduce mechanical properties and dimensional stability. Therefore, balancing water absorption and area expansion is an important problem to be solved [31,32]. Figure 6a,b show the results of water absorption and area expansion, respectively. At each given temperature, samples were immersed in water for 24 h to reach absorption equilibrium before testing. Compared with PFSA pristine membrane, the water uptaking and area

swelling ratio of PFSA@PAN decreased. At 80 °C, compared with PFSA, the area swelling of PFSA@PAN was reduced by 8.3%. This significant decrease can be explained by the following reasons: (i) the combination of PAN and PFSA reduced the proportion of hydrophilic functional groups on PFSA; (ii) PAN effectively inhibited the water uptaking of PFSA@PAN. However, a severe reduction in water content will reduce the efficiency of proton conduction. In order to improve the proton conductivity, in situ synthetic TpPa-SO_3H was used to coat the surface of the nanofibers. After the introduction of TpPa-SO_3H into PFSA, the area swelling of all PFSA@PAN/TpPa-SO_3H membranes was still lower than that of PFSA, but the introduction of a large number of sulfonate groups increased the area swelling of PFSA@PAN. The results showed that adding PAN/TpPa-SO_3H to PFSA may be an excellent solution to balance water absorption and area expansion.

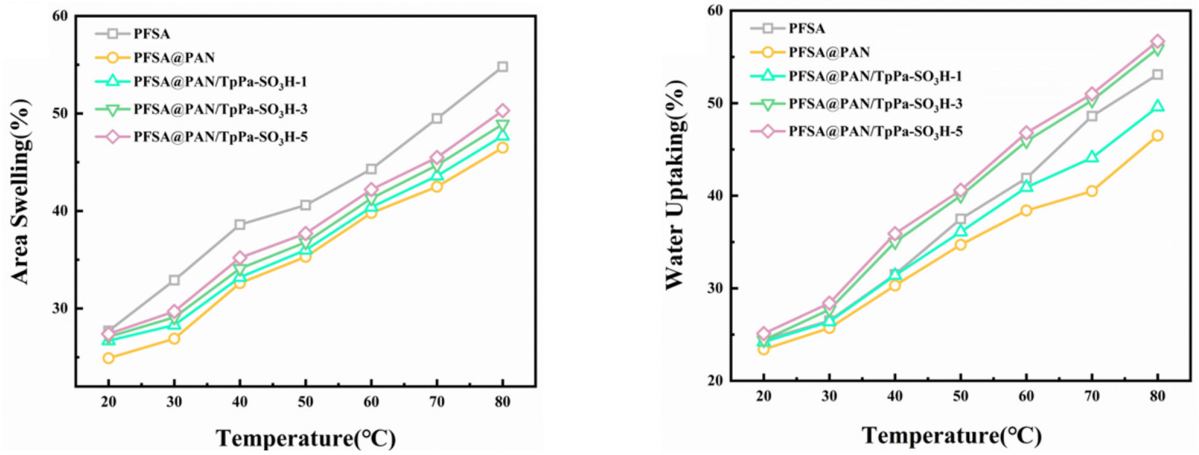

(**a**) (**b**)

Figure 6. (**a**) Area swelling and (**b**) water uptaking of membranes at 100% RH from 20 °C to 80 °C.

3.4. Proton Conductivities

Proton conductivity is an important property for evaluating PEM performance [33]. Figure 7 depicted the proton conductivity of composite membranes at 100% RH under 20~80 °C. Obviously, PFSA@PAN/TpPa-SO_3H-5 showed the highest conductivities at each given temperature. At 80 °C, the proton conductivity of PFSA was 190.83 mS·cm^{-1}, and that of PFSA@PAN was 172.73 mS·cm^{-1}. The proton conductivity of PFSA@PAN/TpPa-SO_3H-5 was 260.81 mS·cm^{-1}, which was about 69.98 mS·cm^{-1} and 88.08 mS·cm^{-1} higher than that of PFSA and PFSA@PAN, respectively. This result showed that PAN/TpPa-SO_3H has enhanced proton conductivities. Furthermore, the stabilities of proton conductivity were tested at 80 °C and 100% RH. The proton conductivity of pristine PFSA membrane decreased from 258.0 mS·cm^{-1} to 209.0 mS·cm^{-1}, and decreased by 19.0% in 264 h. The proton conductivity of the PFSA@PAN composite membrane prepared by adding PAN nanofibers decreased by only 10.8%. The proton conductivity stability of PFSA@PAN/TpPa-SO_3H-5 composite membrane with the highest proton conductivity was also the highest, and the proton conductivity only decreased by 4.7%. The addition of TpPa-SO_3H significantly improved the stability of proton conductivities of composite membranes.

3.5. Thermal Stability, Mechanical Properties and Oxidation Stability Characterization

TGA was performed to characterize the thermal stability of PFSA@PAN/TpPa-SO_3H. As shown in Figure 8a, at temperatures below 220 °C, residual glycol and water will evaporate and cause weight loss. When the temperature is in the range of 280–350 °C, the weight loss is caused by the decomposition of -SO_3H. When the temperature is lower than 300 °C, composite membranes and PFSA show excellent thermal stability [32]. When the temperature is higher than 300 °C, PAN carbonizes in nitrogen atmosphere, resulting in mass loss. When the temperature reaches 400 °C, PFSA and TpPa-SO_3H begin to degrade. TGA showed great thermal stability of the composite membranes.

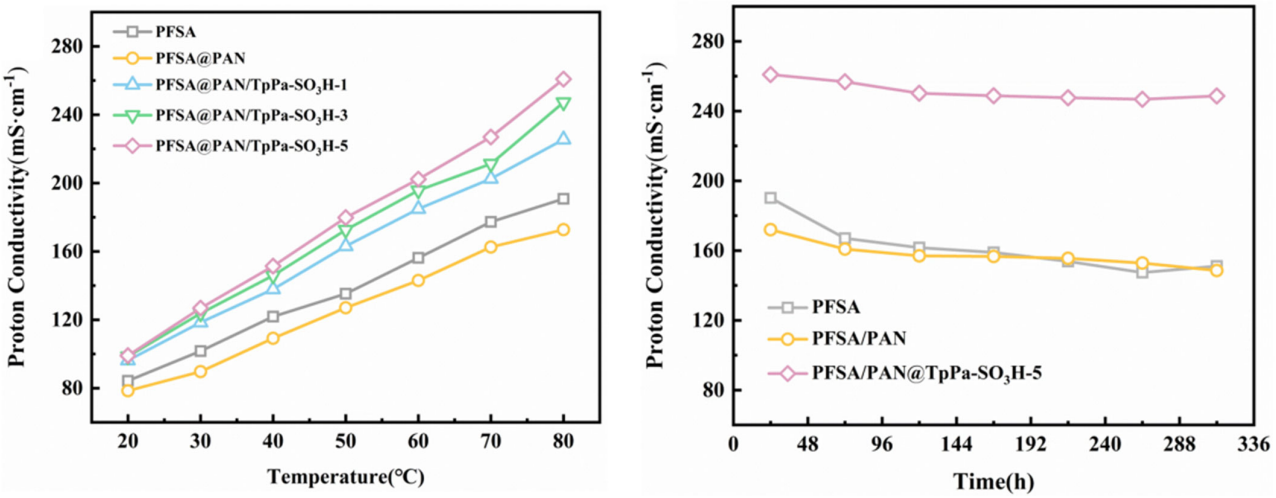

(**a**) (**b**)

Figure 7. (**a**) Proton conductivities of membranes at 100% RH from 20 °C to 80 °C; and (**b**) proton conductivity stability of membranes at 100% RH and 80 °C.

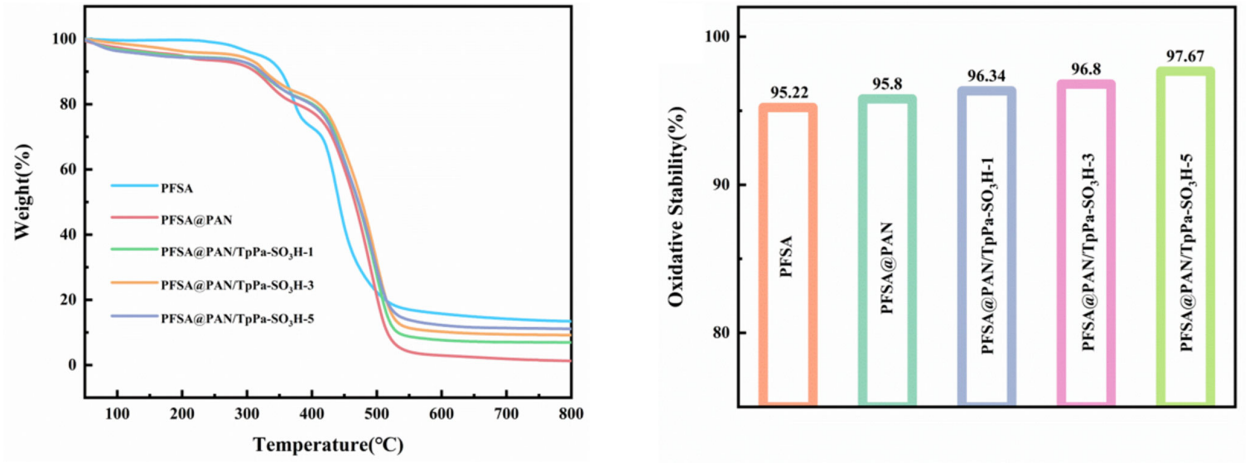

(**a**) (**b**)

Figure 8. (**a**) Thermal stability of PFSA and fibrous composite membranes; (**b**) oxidative stability of PFSA, PFSA@PAN and PFSA@PAN/TpPa-SO_3H composite membranes.

Evaluation of oxidative stability is of vital importance for membranes [34]. The residual mass fractions of membranes after soaking in Fenton's reagent for 24 h at 80 °C are shown in Figure 8b. After soaking in an oxidizing environment for 24 h, the remaining weight of PFSA was 95.22%. The maximum residual mass of fiber composite membranes was 97.67%. Therefore, PAN and PAN/TpPa-SO_3H can enhance the oxidative stability of the membranes.

Figure 9 shows that the addition of PAN/TpPa-SO_3H can significantly improve the tensile strength of composite membranes. In particular, the tensile strength of the PFSA@PAN/TpPa-SO_3H-5 membrane can reach 22.6 MPa. Among all composite membranes, the tensile strength of PFSA@PAN was 17.8 MPa, which was 17.9% higher than that of PFSA, and the elongation at break decreased slightly. Compared with the PFSA, the tensile strength of PFSA@PAN/TpPa-SO_3H composite membranes with different TpPa-SO_3H loadings increased from 9.0% to 27.0%. This phenomenon may be attributed to following reasons: (i) the enhanced electrostatic interaction between-SO_3H (PFSA) and N-H (PAN/TpPa-SO_3H), (ii) the highly continuous fiber network hindered the movement of the ionomer, which weakened the mobility of the PFSA molecular chain and improved

the structural stability of composite membranes. Therefore, the construction of PAN/TpPa-SO_3H nanofibers can optimize the mechanical properties of membranes.

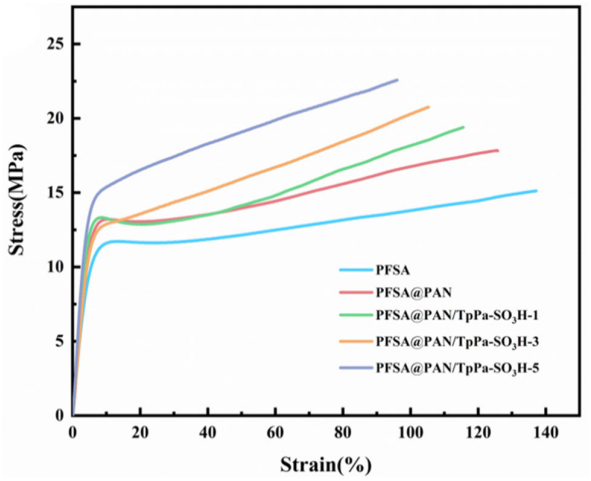

Figure 9. Mechanical property of membranes at 25 °C.

3.6. Fuel Cell Performance

Considering the comprehensive performance of the membranes, PFSA@PAN/TpPa-SO_3H-5 was selected for the fuel cell performance test. The cell performance of PFSA was also measured for comparison (Figure 10). Fuel cell performance was performed at 80 °C and 100% RH. The thicknesses of membranes used in the test were all about 150 µm. The maximum power density of a single fuel cell with of PFSA@PAN/TpPa-SO_3H-5 is 392.7 mW·cm^{-2}, whereas that of PFSA is 350.0 mW·cm^{-2}. This result indicates that the addition of PAN/TpPa-SO_3H to PFSA can improve the performance of fuel cells.

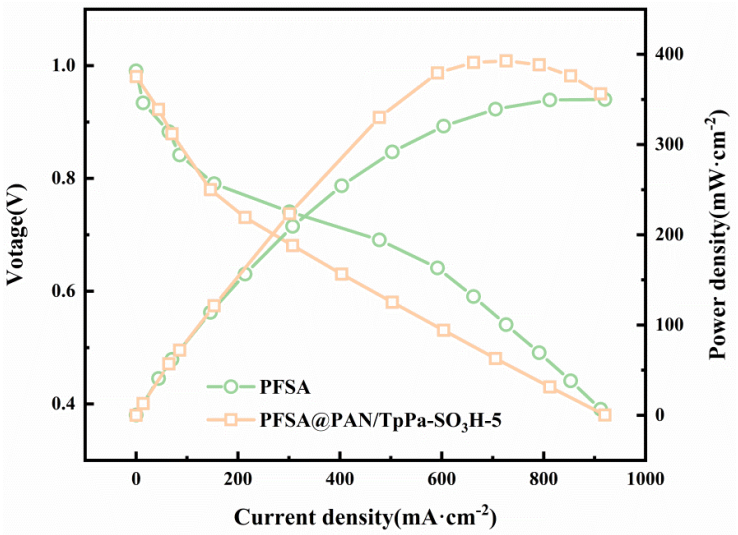

Figure 10. Fuel cell performance characterization of PFSA, and PFSA@PAN/TpPa-SO_3H composite membrane.

4. Conclusions

In conclusion, we proposed a novel strategy to uniformly grow TpPa-SO_3H on the surface of PAN using an in situ synthesis method in order to take full advantage of the three-dimensional network of PAN and to construct continuous and long-range proton conducting channels. As expected, the PFSA@PAN/TpPa-SO_3H-5 composite membrane exhibited better proton conductivity, which could reach 260.81 mS·cm^{-1} at 80 °C and 100% RH, which was about 69.98 mS·cm^{-1} and 88.08 mS·cm^{-1} higher than that of PFSA and PFSA@PAN, respectively, and only decreased by 4.7% in 264 h. Meanwhile, compared with PFSA, the area swelling ratio of PFSA@PAN/TpPa-SO_3H decreased by 7.1%.

In addition, the power density of a single fuel cell with a PFSA@PAN/TpPa-SO_3H-5 composite membrane is as high as 392.7 $mW \cdot cm^{-2}$. All these results suggest that the PFSA@PAN/TpPa-SO_3H composite membranes have the potential to be a promising PEMs for fuel cells.

Author Contributions: Conceptualization, X.M. and Y.L.; methodology, X.M., Y.L. and X.L.; validation, X.M., Y.L., J.W., X.L. and L.P.; formal analysis, X.M., Y.L., J.W. and X.L.; investigation, X.M., Y.L., J.W., X.L. and L.P.; writing—original draft preparation, Y.L.; writing—review and editing, X.M.; Y.L., X.L., L.P., C.C., H.Y. and Q.Z.; supervision, X.M. All authors have read and agreed to the published version of the manuscript.

Funding: This research received no external funding.

Institutional Review Board Statement: Not applicable.

Informed Consent Statement: Not applicable.

Data Availability Statement: The data presented in this study are available on request from the corresponding author.

Acknowledgments: This project was financially supported by Science Foundation of China University of Petroleum, Beijing (No. 2462020YXZZ019).

Conflicts of Interest: The authors declare no conflict of interest.

References

1. Pethaiah, S.S.; Sadasivuni, K.K.; Jayakumar, A.; Ponnamma, D.; Tiwary, C.S.; Sasikumar, G. Methanol electrolysis for hydrogen production using polymer electrolyte membrane: A mini-review. *Energies* **2020**, *13*, 5879. [CrossRef]
2. Li, X.; dos Santos, A.R.; Drache, M.; Ke, X.; Gohs, U.; Turek, T.; Becker, M.; Kunz, U.; Beuermann, S. Polymer electrolyte membranes prepared by pre-irradiation induced graft copolymerization on ETFE for vanadium redox flow battery applications. *J. Membr. Sci.* **2017**, *524*, 419–427. [CrossRef]
3. Kondratenko, M.S.; Karpushkin, E.A.; Gvozdik, N.A.; Gallyamov, M.O.; Stevenson, K.J.; Sergeyev, V.G. Influence of aminosilane precursor concentration on physicochemical properties of composite Nafion membranes for vanadium redox flow battery applications. *J. Power Sources* **2017**, *340*, 32–39. [CrossRef]
4. Wong, C.; Wong, W.; Ramya, K.; Khalid, M.; Loh, K.; Daud, W.; Lim, K.; Walvekar, R.; Kadhum, A. Additives in proton exchange membranes for low-and high-temperature fuel cell applications: A review. *Int. J. Hydrogen Energy* **2019**, *44*, 6116–6135. [CrossRef]
5. Ballengee, J.B.; Pintauro, P.N. Composite fuel cell membranes from dual-nanofiber electrospun mats. *Macromolecules* **2011**, *44*, 7307–7314. [CrossRef]
6. Cavaliere, S.; Subianto, S.; Savych, I.; Jones, D.J.; Rozière, J. Electrospinning: Designed architectures for energy conversion and storage devices. *Energy Environ. Sci.* **2011**, *4*, 4761–4785. [CrossRef]
7. Li, Y.; Hui, J.; Kawchuk, J.; O'Brien, A.; Jiang, Z.; Hoorfar, M. Composite membranes of PVDF nanofibers impregnated with Nafion for increased fuel concentrations in direct methanol fuel cells. *Fuel Cells* **2019**, *19*, 43–50. [CrossRef]
8. Wu, B.; Pan, J.; Ge, L.; Wu, L.; Wang, H.; Xu, T. Oriented MOF-polymer composite nanofiber membranes for high proton conductivity at high temperature and anhydrous condition. *Sci. Rep.* **2014**, *4*, 4334. [CrossRef]
9. Kakade, M.V.; Givens, S.; Gardner, K.; Lee, K.H.; Chase, D.B.; Rabolt, J.F. Electric field induced orientation of polymer chains in macroscopically aligned electrospun polymer nanofibers. *J. Am. Chem. Soc.* **2007**, *129*, 2777–2782. [CrossRef]
10. Fennessey, S.F.; Farris, R.J. Fabrication of aligned and molecularly oriented electrospun polyacrylonitrile nanofibers and the mechanical behavior of their twisted yarns. *Polymer* **2004**, *45*, 4217–4225. [CrossRef]
11. Sood, R.; Cavaliere, S.; Jones, D.J.; Rozière, J. Electrospun nanofibre composite polymer electrolyte fuel cell and electrolysis membranes. *Nano Energy* **2016**, *26*, 729–745. [CrossRef]
12. Yu, D.M.; Yoon, S.; Kim, T.-H.; Lee, J.Y.; Lee, J.; Hong, Y.T. Properties of sulfonated poly (arylene ether sulfone)/electrospun nonwoven polyacrylonitrile composite membrane for proton exchange membrane fuel cells. *J. Membr. Sci.* **2013**, *446*, 212–219. [CrossRef]
13. Liu, G.; Tsen, W.-C.; Jang, S.-C.; Hu, F.; Zhong, F.; Liu, H.; Wang, G.; Wen, S.; Zheng, G.; Gong, C. Mechanically robust and highly methanol-resistant sulfonated poly (ether ether ketone)/poly (vinylidene fluoride) nanofiber composite membranes for direct methanol fuel cells. *J. Membr. Sci.* **2019**, *591*, 117321. [CrossRef]
14. Park, J.W.; Wycisk, R.; Pintauro, P.N. Nafion/PVDF nanofiber composite membranes for regenerative hydrogen/bromine fuel cells. *J. Membr. Sci.* **2015**, *490*, 103–112. [CrossRef]
15. Tanaka, M.; Takeda, Y.; Wakiya, T.; Wakamoto, Y.; Harigaya, K.; Ito, T.; Tarao, T.; Kawakami, H. Acid-doped polymer nanofiber framework: Three-dimensional proton conductive network for high-performance fuel cells. *J. Power Sources* **2017**, *342*, 125–134. [CrossRef]

16. Zhao, G.; Xu, X.; Shi, L.; Cheng, B.; Zhuang, X. Bio-analogue L-lysine lined arrangement on nanofibers with superior proton-conduction for proton exchange membrane. *Solid State Ion.* **2020**, *348*, 115289. [CrossRef]
17. Zhao, G.; Xu, X.; Zhao, H.; Shi, L.; Zhuang, X.; Cheng, B.; Yin, Y. Zeolitic imidazolate framework decorated on 3D nanofiber network towards superior proton conduction for proton exchange membrane. *J. Membr. Sci.* **2020**, *601*, 117914. [CrossRef]
18. Yuan, S.; Li, X.; Zhu, J.; Zhang, G.; Van Puyvelde, P.; Van der Bruggen, B. Covalent organic frameworks for membrane separation. *Chem. Soc. Rev.* **2019**, *48*, 2665–2681. [CrossRef]
19. Sun, Q.; Tang, Y.; Aguila, B.; Wang, S.; Xiao, F.S.; Thallapally, P.K.; Al-Enizi, A.M.; Nafady, A.; Ma, S. Reaction environment modification in covalent organic frameworks for catalytic performance enhancement. *Angew. Chem. Int. Ed.* **2019**, *58*, 8670–8675. [CrossRef]
20. Ji, W.; Xiao, L.; Ling, Y.; Ching, C.; Matsumoto, M.; Bisbey, R.P.; Helbling, D.E.; Dichtel, W.R. Removal of GenX and perfluorinated alkyl substances from water by amine-functionalized covalent organic frameworks. *J. Am. Chem. Soc.* **2018**, *140*, 12677–12681. [CrossRef]
21. Cui, D.; Perepichka, D.F.; MacLeod, J.M.; Rosei, F. Surface-confined single-layer covalent organic frameworks: Design, synthesis and application. *Chem. Soc. Rev.* **2020**, *49*, 2020–2038. [CrossRef] [PubMed]
22. Yin, Y.; Li, Z.; Yang, X.; Cao, L.; Wang, C.; Zhang, B.; Wu, H.; Jiang, Z. Enhanced proton conductivity of Nafion composite membrane by incorporating phosphoric acid-loaded covalent organic framework. *J. Power Sources* **2016**, *332*, 265–273. [CrossRef]
23. Fan, C.; Wu, H.; Li, Y.; Shi, B.; He, X.; Qiu, M.; Mao, X.; Jiang, Z. Incorporating self-anchored phosphotungstic acid@ triazole-functionalized covalent organic framework into sulfonated poly (ether ether ketone) for enhanced proton conductivity. *Solid State Ion.* **2020**, *349*, 115316. [CrossRef]
24. Yao, J.; Xu, G.; Zhao, Z.; Guo, J.; Li, S.; Cai, W.; Zhang, S. An enhanced proton conductivity and reduced methanol permeability composite membrane prepared by sulfonated covalent organic nanosheets/Nafion. *Int. J. Hydrog. Energy* **2019**, *44*, 24985–24996. [CrossRef]
25. Wu, G.; Li, Y.; Geng, Y.; Jia, Z. In situ preparation of COF-LZU1 in poly (ether-block-amide) membranes for efficient pervaporation of n-butanol/water mixture. *J. Membr. Sci.* **2019**, *581*, 1–8. [CrossRef]
26. Yin, Z.; Geng, H.; Yang, P.; Shi, B.; Fan, C.; Peng, Q.; Wu, H.; Jiang, Z. Improved proton conduction of sulfonated poly (ether ether ketone) membrane by sulfonated covalent organic framework nanosheets. *Int. J. Hydrog. Energy* **2021**, *46*, 26550–26559. [CrossRef]
27. Sasmal, H.S.; Aiyappa, H.B.; Bhange, S.N.; Karak, S.; Halder, A.; Kurungot, S.; Banerjee, R. Superprotonic conductivity in flexible porous covalent organic framework membranes. *Angew. Chem.* **2018**, *130*, 11060–11064. [CrossRef]
28. Dey, K.; Pal, M.; Rout, K.C.; Kunjattu, H.S.; Das, A.; Mukherjee, R.; Kharul, U.K.; Banerjee, R. Selective molecular separation by interfacially crystallized covalent organic framework thin films. *J. Am. Chem. Soc.* **2017**, *139*, 13083–13091. [CrossRef]
29. Kandambeth, S.; Mallick, A.; Lukose, B.; Mane, M.V.; Heine, T.; Banerjee, R. Construction of crystalline 2D covalent organic frameworks with remarkable chemical (acid/base) stability via a combined reversible and irreversible route. *J. Am. Chem. Soc.* **2012**, *134*, 19524–19527. [CrossRef]
30. Di Noto, V.; Piga, M.; Giffin, G.A.; Vezzu, K.; Zawodzinski, T.A. Interplay between mechanical, electrical, and thermal relaxations in nanocomposite proton conducting membranes based on nafion and a [(ZrO2)·(Ta2O5) 0.119] core–shell nanofiller. *J. Am. Chem. Soc.* **2012**, *134*, 19099–19107. [CrossRef]
31. Cao, L.; Wu, H.; Cao, Y.; Fan, C.; Zhao, R.; He, X.; Yang, P.; Shi, B.; You, X.; Jiang, Z. Weakly Humidity-Dependent Proton-Conducting COF Membranes. *Adv. Mater.* **2020**, *32*, 2005565. [CrossRef] [PubMed]
32. Chandra, S.; Kundu, T.; Dey, K.; Addicoat, M.; Heine, T.; Banerjee, R. Interplaying intrinsic and extrinsic proton conductivities in covalent organic frameworks. *Chem. Mater.* **2016**, *28*, 1489–1494. [CrossRef]
33. So, S.Y.; Hong, Y.T.; Kim, S.C.; Lee, S.-Y. Control of water-channel structure and state of water in sulfonated poly (arylene ether sulfone)/diethoxydimethylsilane in situ hybridized proton conductors and its influence on transport properties for DMFC membranes. *J. Membr. Sci.* **2010**, *346*, 131–135. [CrossRef]
34. Wycisk, R.; Pintauro, P.N.; Park, J.W. New developments in proton conducting membranes for fuel cells. *Curr. Opin. Chem. Eng.* **2014**, *4*, 71–78. [CrossRef]